

Received 16 June 2024, accepted 27 June 2024, date of publication 18 July 2024, date of current version 29 July 2024.

Digital Object Identifier 10.1109/ACCESS.2024.3430034

RESEARCH ARTICLE

A Phase-to-Phase Protection Algorithm With the Transient Information for the Wind Power Plant Transmission Line

LEI LI¹, JIANAN HE¹, JIAN NIU¹, HAITAO LIU¹, XIAOJUN YU², YING HUANG³,
AND XU ZHANG¹

¹State Grid Ningxia Electric Power Company Ltd., Electric Power Science Research Institute, Yinchuan 750011, China

²State Grid Ningxia Electric Power Company Ltd., Ningxia Power Supply Company, Yinchuan 750001, China

³State Grid Ningxia Electric Power Company Ltd., Yinchuan Power Supply Company, Yinchuan 750001, China

⁴China University of Mining and Technology-Beijing, Beijing 100083, China

Corresponding author: Xu Zhang (zhangxuabb@163.com)


This work was supported by the Technology Project Funding from State Grid Ningxia Electric Power Company Ltd. under Grant 5229DK230003.

ABSTRACT Due to the distinctive fault characteristics of wind power converters in large-capacity wind farms (WFs) with power converter-based systems, protective relays for the connected transmission lines can malfunction, which poses a serious challenge to the stable and reliable power transmission. This article focuses on addressing this issue by proposing a phase-to-phase fault protection method that utilizes single-end transient information for wind farm transmission lines. Conventional solutions often encounter difficulties such as the negative influence of fault resistance and the uncertainty of remote parameters in single-ended data locations. The proposed method employs time-domain differential equations to accurately solve the fault location problem. It takes into account the equivalent resistance and inductance of the transmission line, as well as the fault path resistance. This helps minimize the adverse effects of fault resistance and parameter uncertainties, making the method insensitive to fault impedance and system parameters. The effectiveness of the proposed scheme is comprehensively evaluated using the Real-Time Lab (RTLAB). Various factors like fault resistances, locations, and distributed capacitance are considered. The results clearly demonstrate that the proposed algorithm not only operates at high speed but also exhibits remarkable reliability, offering a promising solution for enhancing the protection of wind farm transmission lines.

INDEX TERMS Fault location, phase-to-phase fault, wind farm, transient information.

I. INTRODUCTION

In order to cope with the problems of energy depletion and environmental pollution, there is an urgent need to change the energy structure, and renewable energy has become the focus of attention. Wind power has become one of the world's most rapidly developing energy sources due to its environmentally friendly and renewable characteristics. As an essential channel for delivering clean energy, the field station delivery line

The associate editor coordinating the review of this manuscript and approving it for publication was Diego Bellan .

must be addressed for the safe and stable operation of the power grid [1], [2], [3]. The traditional relay protection and fault-ranging methods utilized on the sending line need to be better considered, and the current research results need to adequately meet the relay protection requirements after a large amount of wind power is connected to the grid. There are fewer studies on fault ranges in the sending line. Therefore, research on relay protection and fault-ranging methods adapted to wind power stations after grid access is critical to enhance the capacity for green power consumption. It is essential to develop new algorithms, models,

and techniques to improve the accuracy and speed of fault location.

Fault location methods can be divided into three principal categories: artificial intelligence-based, traveling wave-based, and impedance-based. Intelligent algorithms have been applied to fault location in power systems, usually combined with signal processing methods to extract discriminative features. Reference [1] uses support vector machines and discrete wavelet transform to determine the fault part and half. Reference [2] proposes a method based on artificial neural networks (ANN). Reference [3] uses wavelet filtering, protons preprocessing, and artificial neural network localization methods for fault localization. However, it requires high-quality measurements and training data, usually obtained through simulation. In practice, it is difficult to establish a high-fidelity simulation model, so the effectiveness of the results is limited. In addition, these learning algorithms are limited by the input space dimension and may encounter difficulties when using many latent features (such as high-frequency components).

The fault localization method based on a single-ended traveling wave utilizes the arrival time difference between the initial traveling wave and the reflected wave or the arrival time difference between the aircraft model traveling wave and the ground model traveling wave for fault localization [4]. These methods expose high sampling requirements, significant noise impact, reflection wave detection, and wave velocity measurement [5], [6]. In addition, these algorithms also have issues estimating close-range faults and distinguishing whether the second initial traveling wave is reflected from the fault point or from the far end, which significantly limits their adaptability and effectiveness.

Impedance-based methods have the advantages of clear physical meaning, low sampling rate, and simple algorithms and have been widely used in practical power systems. According to different data sources, model-based methods can be divided into single and dual-ended methods. The dual-ended method uses data from both ends, which can effectively offset the impact of changes in line parameters on fault location accuracy [7]. However, these methods require synchronization of measurement data and communication channels for data exchange between terminals.

Some asynchronous algorithms [8], [9] can calculate or eliminate synchronization angles when dual-end data is not synchronized. However, single-ended methods have significant advantages in some cases, such as when there is no communication channel at the remote end or when measurement equipment malfunctions [10]. It has the advantages of cost-effectiveness, simplicity, and compatibility with existing monitoring systems. They aim to find a solution to reduce the impact of fault resistance and unknown faults caused by dual terminal currents. Reference [11] uses negative sequence current to simulate fault current.

In contrast, [12] uses an iterative algorithm to approximate the current after the fault point, assuming that the currents at both ends of the fault point are consistent. Reference [13]

uses a simplified line model in the phase domain and Fast Fourier Transform (FFT) to extract the amplitude and phase of the measured voltage and current at a specific frequency based on the assumption of constant fault resistance. In [14], compensating current is used to reduce the negative impact of fault resistance. In summary, these methods reduce but cannot eliminate the influence of fault resistance and unknown fault current on fault localization.

In addition, high-speed tripping technology makes it difficult to improve the accuracy of the phase domain method. Therefore, finding a fault analysis method based on time-domain transient data is crucial. In order to solve the voltage and current distribution in the time domain, existing methods are usually based on Bergeron models [7], [15], [16], [17], [18], [19], [20], [21] or numerical solutions based on telegraph equations. References [7] and [17] used the characteristic method to solve the telegraph equation numerically. The Bergeron model assumes a lumped series resistor, which introduces errors and accuracy affected by sampling frequency and transmission time [18], [19], [20], [21], [22], [23], [24], [25], [26]. However, the current methods of using transient data and time-domain models are based on dual terminal data, and there are no reports on fault localization based on single terminal transient signals [27], [28], [29], [30], [31], [32], [33], [34], [35].

In order to overcome the problems of the existing single-ended location method and transient signal analysis, this paper focuses on the study of the fault characteristics of large-scale doubly-fed wind power connected to the power system, as well as the existing MV collector lines, high-voltage transmission line protection methods, for large-scale wind farms, the complex collector system structure and protection technology, the difficulties of long-distance transmission line protection technology, in the basis of existing protection methods to seek a new solution to protection methods. A new solution to the protection method is proposed. A phase-to-phase fault location method based on single-ended transient information is proposed, which introduces the commutation resistance pair to more comprehensively consider the actual fault situation. The single-ended voltage and current data are used to obtain the calculation method of phase-to-phase fault location, which does not need the opposite side information, is not affected by the system operation mode, and is highly practical.

In this article, a phase-to-phase fault locating method for the wind farm transmission line with the single end transient information is proposed. A summary of the originality and primary contributions of this study is given below.

- 1) The proposed algorithm is realized in the hardware of the relay for the first time, and the hardware-in-the-loop test platform with RTLAB is developed to verify the method.
- 2) The proposed method can enter the steady state within half cycle, which are faster and more accuracy than the traditional algorithms.

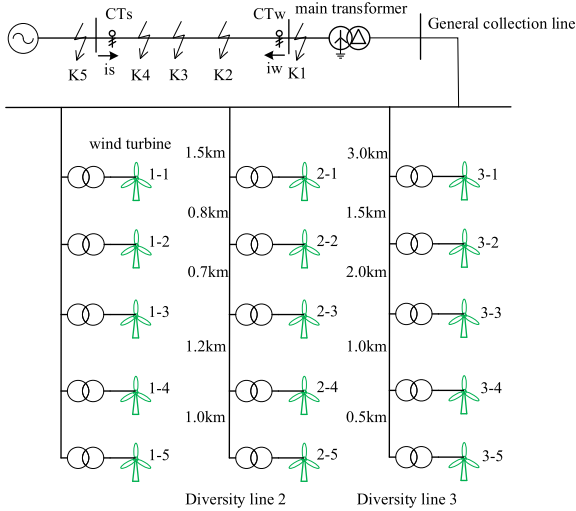


FIGURE 1. Topology of wind farm delivery system.

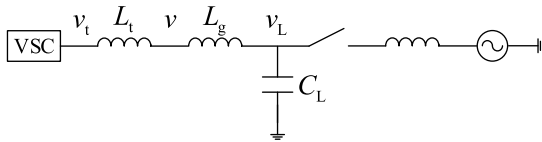


FIGURE 2. Simplified schematic diagram of wind power system.

- 3) the proposed locating method only requires sensors at one measurement point, which reduces the cost of equipment and maintenance and has a higher value for engineering applications.
- 4) The approach i tested for different scenarios simulated by considerin various parameters such as the system impedance ratio, fault distance, and fault resistance that could impact the fault currents. The locating errors were within an acceptable range.

The rest of the paper is structured as follows. In Section II, the phase-to-phase fault protection algorithm for wind farm outgoing lines, which is based on single-end transient information, is described in Section II. In Section III, the single phase-to-phase fault protection method for a wind farm transmission line based on single-end information is verified using RTLAB. In Section IV, a sensitivity analysis of the proposed algorithm is presented. Finally, Section V concludes the paper.

II. PHASE-TO-PHASE PROTECTION METHOD BASED ON THE SINGLE END INFORMATION

A. MODELING OF THE WIND FARM

The topology of a typical wind farm access system is shown in Figure 1, including direct-drive wind turbines, box transformers, collector lines, main transformers of the booster station, reactive power compensation equipment, transmission lines, and others. CTw and CTs are the current transformers on the wind farm side, and the system side of the transmission lines, respectively, and the positive direction of the current is

pointing from the busbar to the line. The grid-side converter, machine-side converter, and chopper circuits of direct-drive WTGs are typically controlled among them. The wind turbine has high- and low-voltage ride-through functions specified in the national standard.

For modeling the simplified wind power delivery system shown in Figure 2, a single turbine represents the wind farm, and a centralized inductance and capacitance represent the transformer and transmission lines. The external inductance and capacitance are converted from the original two-level voltage system, based on the rated capacity of the wind turbine, and calculated using the Mississippi system. Instead of listing the individual line's high reactance, the value of capacitance C_L is discounted according to the actual high reactance compensation degree, thus simulating the working conditions of accessing high reactance of different capacities. In contrast, the line and transformer impedance are incorporated into the L_g calculation.

In order to analyze the load-shedding frequency over-voltage, the direct-drive wind turbine is also modeled in a simplified way. Considering only the inner-loop controller of the grid-side converter, the filter inductor's dynamics, and the system's inductance and capacitance dynamics, an 8th-order simplified model is obtained. The proportional-integral controller equations used for current control are:

$$\begin{cases} x_d = (K_i + \frac{1}{T_{is}})(i_{dRef} - i_d) \\ x_q = (K_i + \frac{1}{T_{is}})(i_{qRef} - i_q) \end{cases} \quad (1)$$

where x_d and x_q are the output variables of the proportional-integral controllers for the d and q axes, respectively; i_d and i_q are the d and q axes currents, respectively, and i_{dRef} and i_{qRef} are the reference values of the d and q axes currents, respectively.

The fan controller equation ignoring the phase-locked loop is:

$$\begin{cases} v_{td}^c = x_d - \omega_0 L_t i_q + 1 \\ v_{tq}^c = x_q + \omega_0 L_t i_d \end{cases} \quad (2)$$

The controller is also configured with two limiting links to ensure a reasonable range of output voltage:

$$\begin{cases} -1 \leq x_d \leq 1 \\ -1 \leq x_q \leq 1 \end{cases} \quad (3)$$

$$\begin{cases} \begin{cases} v_{td}^c = v_{td}^c \\ v_{tq}^c = v_{tq}^c, \end{cases} & \sqrt{(v_{td}^c)^2 + (v_{tq}^c)^2} \leq 1.5 \\ \begin{cases} v_m = 1.5 \\ v_{td}^c = \frac{v_{td}^c}{v_m} \\ v_{tq}^c = \frac{v_{tq}^c}{v_m}, \end{cases} & \sqrt{(v_{td}^c)^2 + (v_{tq}^c)^2} > 1.5 \end{cases} \quad (4)$$

The variables in the formula are calculated using the standardized system, and the limit values of ± 1 and 1.5 are typical engineering values.

Neglecting the dynamic process of PWM, only the saturation characteristics of PWM are considered, the converter output port voltage v_t is considered to be equal to the output voltage v_t^c of Eq. (2) multiplied by the saturation coefficient; at the same time, taking into account the control limiting link of Eq. (3) and Eq. (4), the conversion coefficients K_d and K_q are introduced to get the vector form of the final converter port voltage:

$$v_t = K_d (x_d + 1) + jK_q x_q + j\omega_0 L_t \begin{bmatrix} K_d & 0 \\ 0 & K_q \end{bmatrix} i \quad (5)$$

The dynamic equations of the electrical components in dq coordinates for the normal mode of operation of the wind power delivery system are:

$$\begin{cases} (s + j\omega_0)L_t i = v_t - v \\ [R_g + (s + j\omega_0)L_g]i = v - v_L \\ (s + j\omega_0)C_L v_L = i \end{cases} \quad (6)$$

where v is the voltage at the PCC point, v_L is the voltage on the turbine side of the transmission line, L_t is the filtering inductance of the converter port, L_g is the inductance between the PCC point and the transmission line, and the impedance of the turbine's 35 and 220 kV step-up transformers is incorporated into L_g for consideration. In contrast, the change in the transformer wiring form caused by the change of the sequential network is only simplified and taken into account in the analysis model. The model is mainly used to qualitatively analyze the transient response characteristics of the wind turbine during load shedding. Each electrical component and electrical quantity are shown in Figure 2.

B. A BRIEF DESCRIPTION OF THE PRINCIPLES OF LEAST SQUARES MULTIPLE REGRESSION

Regression analysis examines the relationship between several variables. It examines the relationship between the independent variable x , or set of independent variables $\{x_1, x_2, \dots, x_n\}$, and the dependent variable, y usually for predictive analysis. Generally, the relationship between the independent variables and the dependent variables is divided into linear and non-linear relationships, known as linear regression and non-linear regression respectively. Typically, the independent variable $\{x_1, x_2, \dots, x_m\} (m \geq 2)$ and the dependent variable y form a sample data set $\{x_1, x_2, \dots, x_m, y\} (m+1)*n$ and there is a linear relationship as follows [18]:

$$y = \theta_0 + \theta_1 x_1 + \theta_2 x_2 + \dots + \theta_m x_m + \zeta \quad (7)$$

where $\theta_0, \theta_1, \theta_2, \dots, \theta_m$ is the solution factor; ζ is the residuals.

An equation shaped like equation (7) is a multiple regression:

$$\begin{aligned} \min : Q(\theta_0, \theta_1, \theta_2, \dots, \theta_m) \\ = \sum_{i=1}^n [y_i - (\theta_0 + \theta_1 x_{1i} + \theta_2 x_{2i} + \dots + \theta_m x_{mi})]^2 \end{aligned} \quad (8)$$

Equation (8) is a least-squares estimation, the purpose of which is to find the optimal solution to the multiple regression equation to ensure that the predicted value of the model is closest to the actual value.

C. FAULT LOCATION ALGORITHM

The voltage-current expression for phase-phase faults in columns:

$$\dot{U}_{\varphi\varphi} = Z\dot{I}_{\varphi\varphi} + R_t \dot{I}_{\varphi\varphi}, \dot{U}_{\varphi\varphi} = lZ_1 \dot{I}_{\varphi\varphi} + R_t \dot{I}_{\varphi\varphi} \quad (9)$$

where $\dot{U}_{\varphi\varphi}, \dot{I}_{\varphi\varphi}$ for the protection of the installation measured at the line voltage phase and line current phase quantity; $\Delta \dot{I}_{\varphi\varphi}$ for the line current after the fault and the pre-fault changes in the amount, $\varphi\varphi = AB, BC,$ and $CA,$ respectively, that is, between the phases of AB, BC, or CA; l for the fault distance; Z for the fault line impedance; Z_1 for the fault line unit of the positive-sequence impedance, negative-sequence impedance, and zero-sequence impedance; R_t is the equivalent resistance.

Expanding equation (9) into the time domain gives the following equation:

$$u_{\varphi\varphi} = lr_1 i_{\varphi\varphi} + lL_1 \frac{di_{\varphi\varphi}}{dt} + R_t \Delta i_{\varphi\varphi} \quad (10)$$

where $u_{\varphi\varphi}$ and $i_{\varphi\varphi}$ are the time-domain values of the phase-to-phase voltages and currents at the time of the fault, respectively, and $\Delta i_{\varphi\varphi}$ is the time-domain value of the magnitude of the current change between post-fault and pre-fault.

Define the objective function:

$$E(l, R_t) = \sum_{i=1}^n \left[u_{\varphi\varphi i} - \left(lr_1 i_{\varphi\varphi i} + lL_1 \frac{di_{\varphi\varphi i}}{dt} + R_t \Delta i_{\varphi\varphi i} \right) \right]^2 \quad (11)$$

where $\sum_{i=1}^n$ is the residual sum of squares; $u_{\varphi\varphi i}, i_{\varphi\varphi i},$ and $\Delta i_{\varphi\varphi i}$ denote the phase-phase voltage value, current value, and current change between the post-fault and pre-fault at the i th acquisition, respectively; $i = 1, 2, \dots, n.$

The residual vector and the design matrix are constructed:

$$\vec{R} = \begin{bmatrix} u_{\varphi\varphi 1} - \left(lr_1 i_{\varphi\varphi 1} + lL_1 \frac{di_{\varphi\varphi 1}}{dt} + R_1 \Delta i_{\varphi\varphi 1} \right), \\ u_{\varphi\varphi 2} - \left(lr_1 i_{\varphi\varphi 2} + lL_1 \frac{di_{\varphi\varphi 2}}{dt} + R_1 \Delta i_{\varphi\varphi 2} \right), \\ \dots, \\ u_{\varphi\varphi n} - \left(lr_1 i_{\varphi\varphi n} + lL_1 \frac{di_{\varphi\varphi n}}{dt} + R_1 \Delta i_{\varphi\varphi n} \right) \end{bmatrix} \quad (12)$$

$$X = \begin{bmatrix} \left[- \left(r_1 i_{\varphi\varphi 2} + L_1 \frac{di_{\varphi\varphi 2}}{dt} \right), -\Delta i_{\varphi\varphi 2} \right], \\ \left[- \left(r_1 i_{\varphi\varphi 2} + L_1 \frac{di_{\varphi\varphi 2}}{dt} \right), -\Delta i_{\varphi\varphi 2} \right], \\ \dots, \\ \left[- \left(r_1 i_{\varphi\varphi n} + L_1 \frac{di_{\varphi\varphi n}}{dt} \right), -\Delta i_{\varphi\varphi n} \right] \end{bmatrix} \quad (13)$$

$$\begin{aligned} E = R^T \cdot R = \left[u_{\varphi\varphi} - X \cdot [l, R_t]^T \right]^T \\ \cdot \left[u_{\varphi\varphi} - X \cdot [l, R_t]^T \right] \end{aligned} \quad (14)$$

The partial derivatives of the residual sum of squares can be obtained such that the residual sum of squares reaches a minimum value:

$$\nabla E = \left[\frac{\partial E}{\partial l}, \frac{\partial E}{\partial R_t} \right] = -2X^T \cdot [u_{\varphi\varphi} - X \cdot [l, R_t]^T] = 0 \quad (15)$$

Define the matrix A on the left and the vector B on the right:

$$\begin{aligned} A &= X^T \cdot X \\ B &= X^T \cdot u_{\varphi\varphi} \end{aligned} \quad (16)$$

Then equation. (15) reduces to solving the regular equation:

$$A \cdot [l, R_t]^T = B \quad (17)$$

The values of the parameter vectors can be solved for by matrix inversion:

$$[l, R_t]^T = A^{-1} \cdot B \quad (18)$$

where the parameter vector consists of the distance to the fault of the quantity to be sought l and the equivalent resistance R_t .

If the matrix A is not invertible, perform a singular value decomposition on the matrix X :

$$X = U \cdot \Sigma \cdot V^T \quad (19)$$

where U is an orthogonal matrix, the column vector of U is the eigenvector of $X^T X$; Σ is a singular value diagonal matrix, the elements of Σ which lie on the diagonal are the singular values; said singular values are the square root of the eigenvalues obtained from the singular value decomposition of the matrix X , and V is an orthogonal matrix, the column vector of V is the eigenvector of $X^T X$.

Calculate the pseudoinverse of X :

$$X^+ = V \cdot \Sigma^+ \cdot U^T \quad (20)$$

where Σ^+ denotes the pseudo-inverse of Σ . The diagonal elements are considered as inverses, and the inverse of the nonzero element is placed back on the diagonal.

The pseudo-inverse can be solved for the value of the parameter vector:

$$[l, R_t]^T = X^+ \cdot u_{\varphi\varphi} \quad (21)$$

The flowchart of the fault location algorithm is as follows:

III. SIMULATION VERIFICATION

The test model of the 500 kV wind power transmission line is shown in Figure 4. The detailed parameters for this model are provided in the Appendix. Power system simulation and algorithmic calculations are performed using RTLAB. The hardware-in-the-loop real time platform including the RTLAB and the hardware of the relay is built to test the algorithm. RTLAB was used for the power system simulation, while the hardware of the relay is developed to realize the proposed method.

The studied zone I phase-to-phase distance relay is set to protect 85% of the 200 km transmission line (i.e., 170 km).

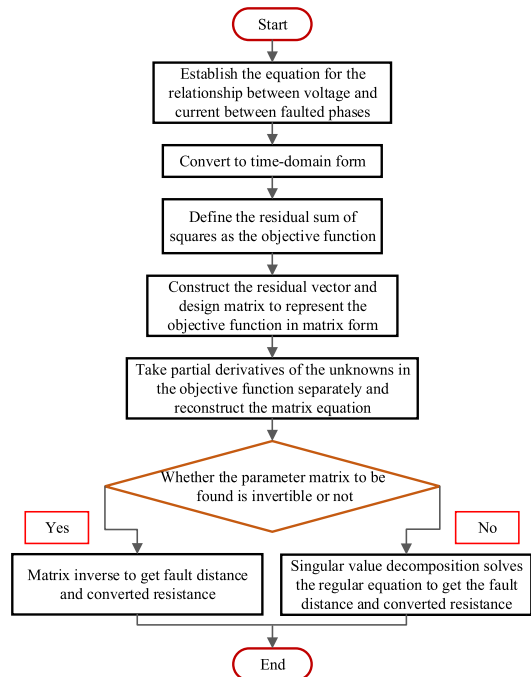


FIGURE 3. The flowchart of the fault location algorithm.

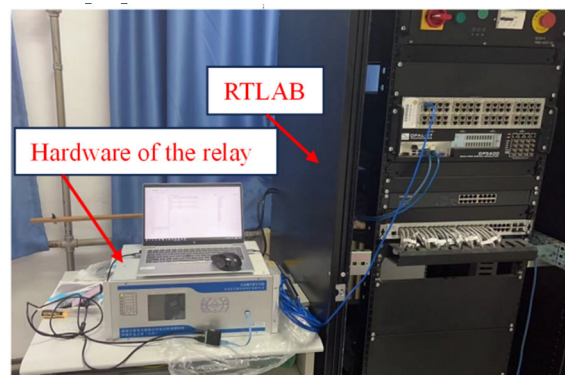


FIGURE 4. The hardware-in-the-loop real time platform.

Source M leads source N at an angle between 0° (no load) and 30° (heavy load), and the fault starts at 0.4 s. A sampling rate of 80 samples per cycle (for a 50 Hz system) is used, and a Butterworth low-pass filter with a cut-off frequency of 120 Hz is selected to filter out the higher harmonic components. The sample rate is 4000Hz.

To validate and evaluate the new algorithm, some comparative results are given between the new algorithm and the traditional distance protection algorithms widely used for the distance protection of transmission lines. The conventional algorithm for phase-to-phase faults is as follows:

$$Z_{\varphi\varphi} = U_{\varphi\varphi} / I_{\varphi\varphi} \quad (22)$$

(1) A phase-to-phase fault occurs inside the critical distance protection. For example, a phase A to B fault occurs in the outgoing line 100 km (50% of the total length of the line)

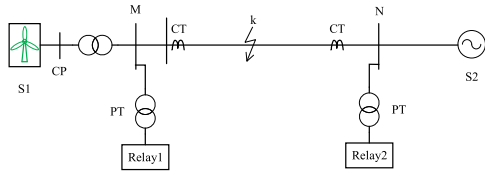


FIGURE 5. Wind farm outgoing line model.

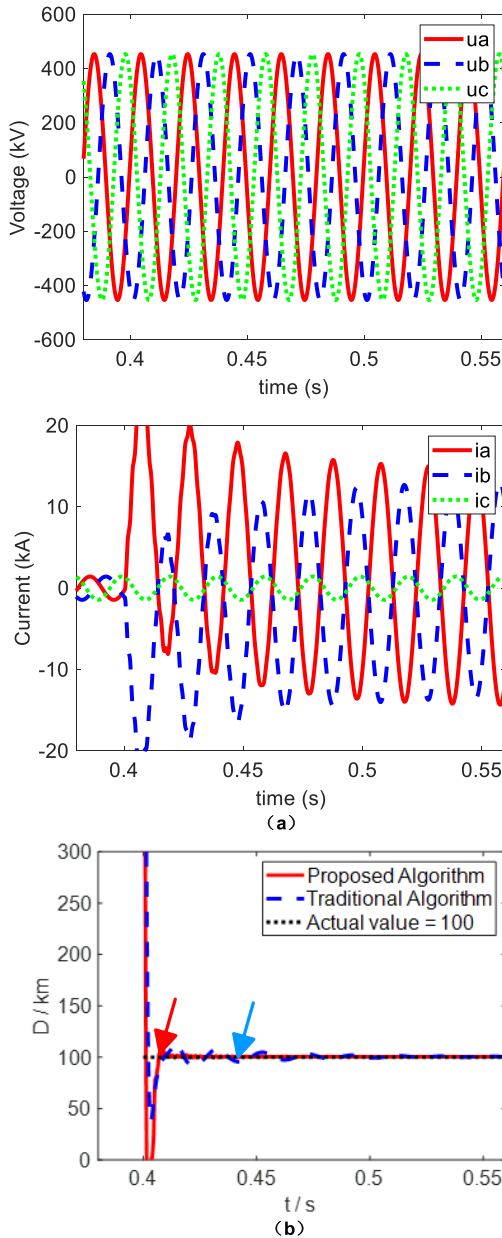


FIGURE 6. Voltage and current waveforms and calculated impedance under a ABG fault 100 km from bus M (a) Voltage and relay voltage waveforms (b) Fault impedance traces measured at terminals M and N.

from bus M. At this point, the transition resistance is 0Ω . As shown in Figure 6(a), the three-phase voltages remain essentially unchanged during the fault, and the currents of phases A and B increase sharply. The proposed algorithm is

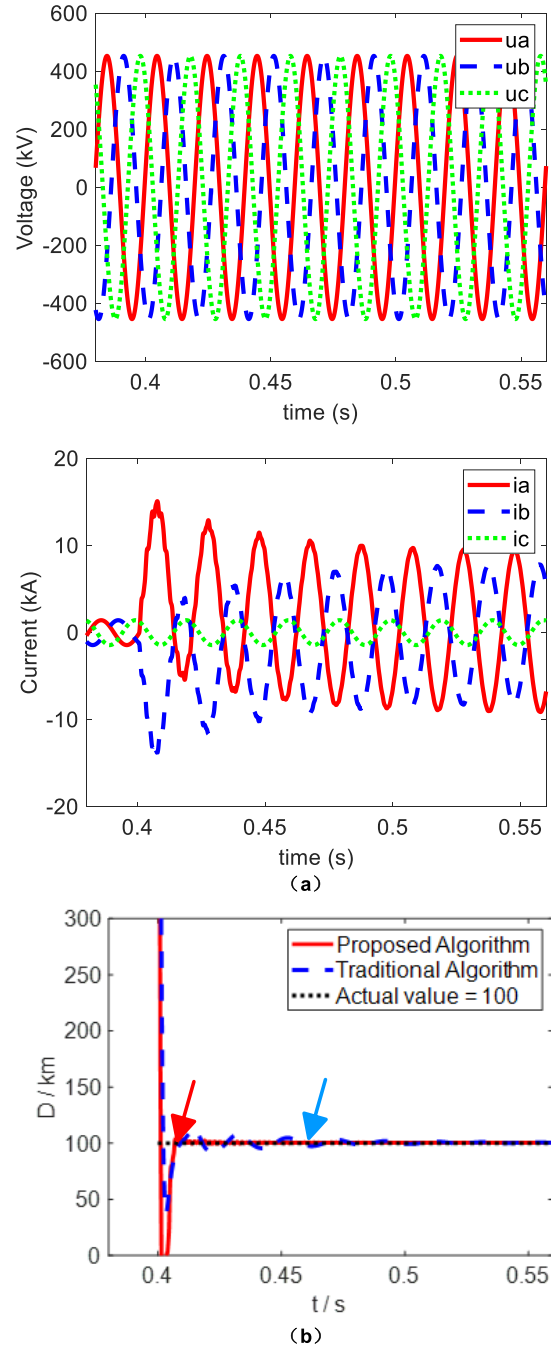


FIGURE 7. Voltage and current waveforms and calculated impedance under ABG fault at 160 km from bus M (a) Relay voltage and voltage waveforms (b) Fault impedance traces measured at terminals M and N.

compared with the distance calculated using the traditional algorithm shown in Figure 6(b), where the data are measured by relays 1 and the measured fault distance(D) is obtained by the quotient of the reactance calculated by the algorithm and the line unit reactance. The proposed algorithm enters the steady state in approximately 7ms, while the conventional algorithm enters the steady state in approximately 40ms, and the proposed algorithm has less error in fault distance measurement.

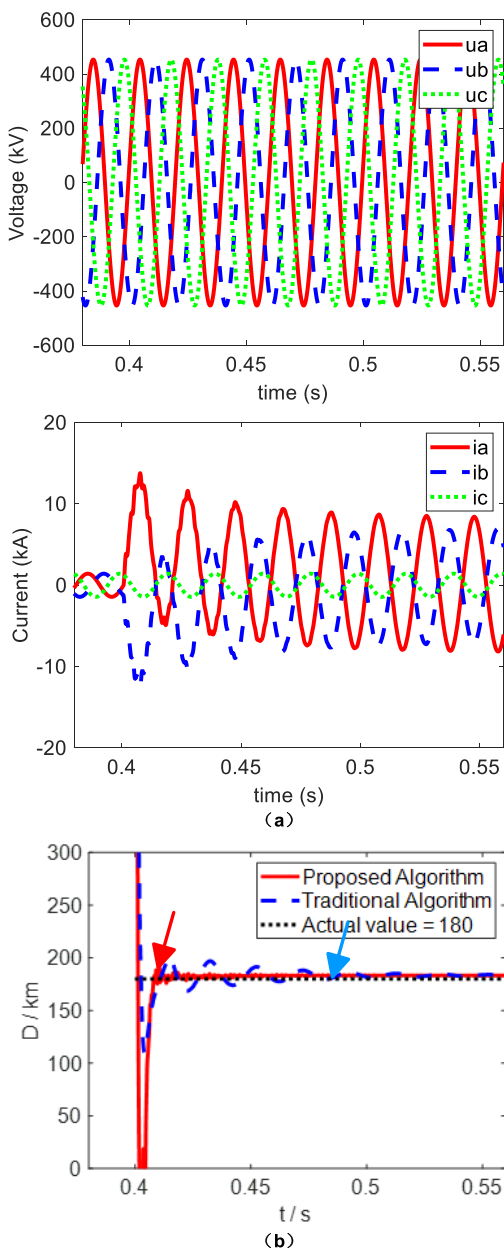


FIGURE 8. Voltage and current waveforms and calculated impedance during an ABG fault at 180 km from bus M (a) Relay voltage and voltage waveforms (b) Fault impedance traces measured at terminals M and N.

(2) A phase-to-phase fault occurs inside the critical distance protection. For example, a phase-to-phase fault occurs in AB of the outgoing line 160 km (80% of the total length of the line) from bus M. At this time, the transition resistance is 0 Ω. As shown in Figure 7(a), the three-phase voltages remain unchanged during the fault, and the currents of phases A and B both increase sharply. The fault distances calculated using the two algorithms are compared in Figure 7(b), and the traditional algorithm enters a steady state in approximately 65ms, while the proposed algorithm enters a steady state in approximately 10ms, which is significantly faster than the traditional algorithm. Meanwhile, the fault

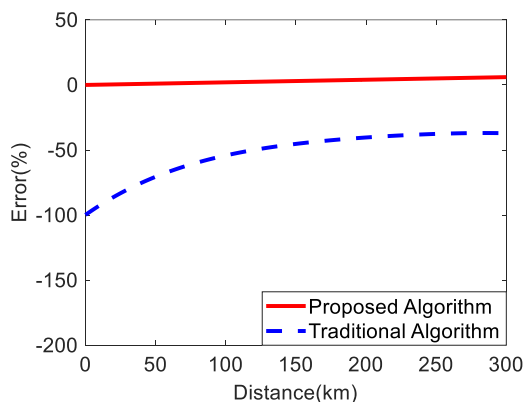


FIGURE 9. Estimated fault reactance error for BCG ground fault at different fault locations for $\delta = 30^\circ$ condition.

distance calculated by the traditional algorithm is almost the same as that of the proposed algorithm. This algorithm can accurately calculate the fault distance.

(3) A phase-to-phase fault occurs inside the critical distance protection. For example, a phase-to-phase fault occurs in AB of the outgoing line 180 km (90% of the total length of the line) from bus M. At this time, the transition resistance is 0 Ω. As shown in Figure 8(a), the three-phase voltages remain unchanged during the fault, and the currents of phases A and B both increase sharply. The fault distances calculated using the two algorithms are compared in Figure 8(b), and the traditional algorithm enters a steady state in approximately 80ms, while the proposed algorithm enters a steady state in approximately 9ms, which is significantly faster than the traditional algorithm. At the same time, traditional algorithm already has obvious errors, and the measured value is larger than the actual value, which may result in the refusal to operate.

The error in calculating the fault reactance is derived using equation (23):

$$E(\%) = \frac{(X - X_a)}{X_a} * 100 \tag{23}$$

where X_a is the actual fault reactance of the line and X is the calculated fault reactance.

To further verify the effectiveness of the new algorithm, it is compared with the traditional algorithm under various typical fault conditions. Figure 9 shows the comparison results between the new algorithm and the traditional algorithm when a BC-phase indirect ground fault occurs in the outgoing line of the wind power base. The faults of $\delta = 30^\circ$ (heavy load, source M leading source N) are simulated at different fault location.

In Figure 9, the error of the new algorithm is significantly smaller than that of the traditional algorithm. In this case, the relay with the new algorithm can operate correctly, whereas the relay with the traditional algorithm may be out of range. As shown in Figure 9, the maximum error of the new algorithm is less than 3.0%, whereas the error of the traditional algorithm reaches 80%. The algorithm suffers

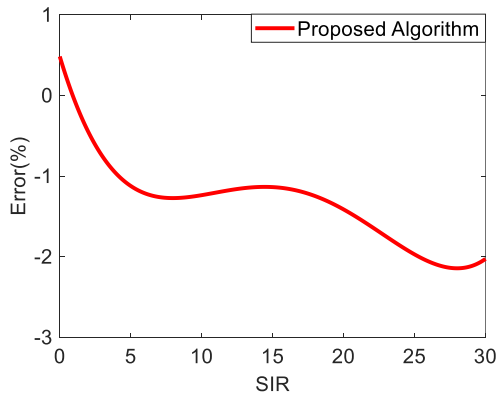


FIGURE 10. Estimated error for a BCG fault at 80% distance from bus.

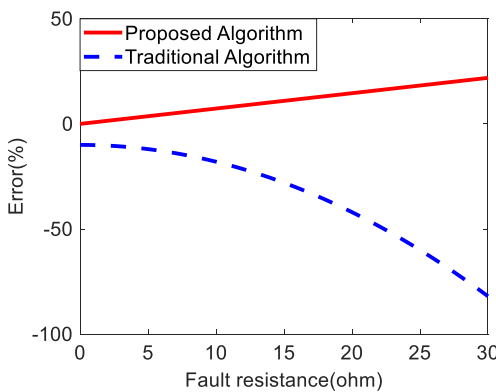


FIGURE 11. Estimated fault reactance error under a CAG fault with a fault resistance of 0–30 Ω at a distance of 150 km from the bus.

from errors because it ignores the shunt capacitance of the transmission line and the test uses a distributed parameter model.

IV. SENSITIVITY ANALYSIS

A. EFFECT OF PARALLEL CAPACITANCE

The algorithm is derived by ignoring the line shunt capacitance. As shown in Figure 6 to Figure 9, a simulation is performed using a distributed parameter line model. The maximum relative error is less than 3.0%. The results show that the error of the algorithm (including the effect of shunt capacitance) is less than 3.0% for a 200 km, 500 kV wind farm transmission line; therefore, the effect of shunt capacitance on the algorithm can be ignored in practical applications.

B. INFLUENCE OF SIR (SYSTEM IMPEDANCE RATIO)

The SIR reflects the ratio of the equivalent impedance of the system to the relay arrival impedance. For wind turbine baseline faults, the smaller the SIR, the higher the fault current, and the higher the resulting equivalent impedance and resistance. The effect of SIR on the proposed algorithm is illustrated in this section. A series of phase-to-phase faults at 80% of the M-end of the outgoing transmission line is simulated at different SIRs. The fault reactance error of the proposed algorithm is illustrated in Figure 10. Figure 10

shows that the proposed algorithm performs well when phase-to-phase faults occur at different SIRs. The simulations are performed under extreme conditions of (series capacitance in line impedance) and (heavy load). As shown in Figure 10, the maximum error of the algorithm is less than $\pm 3\%$; therefore, the effect of the SIR on the algorithm is negligible.

C. EFFECT OF FAULT RESISTANCE AND LOAD CURRENT

From the derived equation, it is clear that the accuracy of the new algorithm is affected by fault resistance and load current. Figure 3–6 show that the new algorithm works perfectly for phase-to-phase faults.

In practice, the resistance of a two-phase fault may be relatively small. Simulations are performed for CA phase-to-phase faults under extreme conditions (high loads) and fault resistances of 0–30 Ω . As shown in Figure 9, the error of the new algorithm is much smaller than that of the conventional algorithm.

V. CONCLUSION

This paper proposes a new single-terminal time-domain fault location approach for quick tripping of wind farm outgoing lines as well as a wide range of power electronic device applications. Unlike previous systems, the method employs fault transient data from a single terminal, avoiding the need to assume unknown distant source impedance and current characteristics on both ends. A numerical derivation approach using least squares multiple regression and algebra is proposed. The equivalent resistance pair is introduced to fully evaluate the real fault scenario, and the phase-to-phase fault distance is calculated using single-ended voltage and current data. The fault-ranging data demonstrate that the approach can properly locate the problem with an inaccuracy of less than 1%. The approach has several advantages, including clear physical interpretation, straightforward computation, and practicality.

Despite the results achieved in this study, there are still some research gaps and future perspectives that deserve further exploration. Firstly, the current method has challenges in dealing with complex network topologies and uncertain parameters, and future research can explore more accurate models and algorithms to improve the applicability and robustness of the algorithm. In addition, the real-time and computational efficiency of the algorithm is also an important research direction, and the algorithm can be further optimized in the future to improve its efficiency and usefulness in practical applications.

APPENDIX

1) Parameters of 200km, 500kV Bergeron Model lines:

Positive/negative sequence parameters:

Positive/negative sequence resistance:

$R = 0.022 \text{ ohm/km}$

Positive/negative sequence inductive reactance:

$XL = 0.28 \text{ ohm/km}$

Positive/negative sequence capacitive reactance:

$X_c = 0.24144 \text{ Mohm} \cdot \text{km}$
 Zero-sequence parameters:
 Zero-sequence resistance: $R_0 = 0.1828 \text{ ohm/km}$
 Zero-sequence inductance: $X_{L0} = 0.86 \text{ ohm/km}$
 Zero-sequence capacitance: $X_{c0} = 0.57875 \text{ Mohm} \cdot \text{km}$
 Mutual zero-sequence parameters:
 Mutual zero-sequence resistance:
 $R_m = 0.000295 \text{ ohm/km}$
 Mutual zero-sequence inductance:
 $X_{Lm} = 0.522 \text{ ohm/km}$
 Mutual zero-sequence capacitance:
 $X_{cm} = 0.98645 \text{ Mohm} \cdot \text{km}$
 System parameters:
 Source M parameters:
 Voltage: 500kV
 2 MW PM parameters:
 Rated voltage: 0.69kV
 Frequency: 50Hz
 Number of turbines: 100
 Resistance: $R = 1.33 \Omega$
 Inductance: $L = 0.621 \text{ mH}$
 Capacitance: $C = 700 \mu\text{F}$
 Source N parameters:
 Voltage: 500kV
 Positive/negative sequence reactance:
 $X_1 = X_2: 9.0 \text{ ohm (min)}, 182.0 \text{ ohm (max)}$
 Zero-sequence reactance:
 $X_0 = 18.2 \text{ ohm (min)}, 364.4 \text{ ohm (max)}$

REFERENCES

- [1] H. Livani and C. Y. Evrenosoglu, "A machine learning and wavelet-based fault location method for hybrid transmission lines," *IEEE Trans. Smart Grid*, vol. 5, no. 1, pp. 51–59, Jan. 2014.
- [2] M. Farshad and J. Sadeh, "Accurate single-phase fault-location method for transmission lines based on K-nearest neighbor algorithm using one-end voltage," *IEEE Trans. Power Del.*, vol. 27, no. 4, pp. 2360–2367, Oct. 2012.
- [3] M. M. Tawfik and M. M. Morcos, "On the use of Prony method to locate faults in loop systems by utilizing modal parameters of fault current," *IEEE Trans. Power Del.*, vol. 20, no. 1, pp. 532–534, Apr. 2005.
- [4] R. Mardiana, H. A. Motairy, and C. Q. Su, "Ground fault location on a transmission line using high-frequency transient voltages," *IEEE Trans. Power Del.*, vol. 26, no. 2, pp. 1298–1299, Apr. 2011.
- [5] M. Majidi and M. Etezadi-Amoli, "A new fault location technique in smart distribution networks using synchronized/nonsynchronized measurements," *IEEE Trans. Power Del.*, vol. 33, no. 3, pp. 1358–1368, Jun. 2018.
- [6] G. Feng and A. Abur, "Fault location using wide-area measurements and sparse estimation," *IEEE Trans. Power Syst.*, vol. 31, no. 4, pp. 2938–2945, Jul. 2016.
- [7] A. Gopalakrishnan, M. Kezunovic, S. M. McKenna, and D. M. Hamai, "Fault location using the distributed parameter transmission line model," *IEEE Trans. Power Del.*, vol. 15, no. 4, pp. 1169–1174, Nov. 2000.
- [8] C.-S. Yu, L.-R. Chang, and J.-R. Cho, "New fault impedance computations for unsynchronized two-terminal fault-location computations," *IEEE Trans. Power Del.*, vol. 26, no. 4, pp. 2879–2881, Oct. 2011.
- [9] Y. Zhang, J. Liang, Z. Yun, and X. Dong, "A new fault-location algorithm for series-compensated double-circuit transmission lines based on the distributed parameter model," *IEEE Trans. Power Del.*, vol. 32, no. 6, pp. 2398–2407, Dec. 2017.
- [10] F. V. Lopes, E. J. S. Leite Jr., J. P. G. Ribeiro, A. B. Piardi, A. V. Scheid, G. Zat, and R. G. F. Espinoza, "Single-ended multi-method phasor-based approach for optimized fault location on transmission lines," *Electr. Power Syst. Res.*, vol. 212, Nov. 2022, Art. no. 108361.
- [11] M.-S. Choi, S.-J. Lee, D.-S. Lee, and B.-G. Jin, "A new fault location algorithm using direct circuit analysis for distribution systems," *IEEE Trans. Power Del.*, vol. 19, no. 1, pp. 35–41, Jan. 2004.
- [12] S.-J. Lee, M.-S. Choi, S.-H. Kang, B.-G. Jin, D.-S. Lee, B.-S. Ahn, N.-S. Yoon, H.-Y. Kim, and S.-B. Wee, "An intelligent and efficient fault location and diagnosis scheme for radial distribution systems," *IEEE Trans. Power Del.*, vol. 19, no. 2, pp. 524–532, Apr. 2004.
- [13] K. Jia, D. Thomas, and M. Sumner, "A new single-ended fault-location scheme for utilization in an integrated power system," *IEEE Trans. Power Del.*, vol. 28, no. 1, pp. 38–46, Jan. 2013.
- [14] R. Živanović, "Evaluation of transmission line fault-locating techniques using variance-based sensitivity measures," in *Proc. 16th Power Syst. Comput. Conf.*, 2008, pp. 15–27.
- [15] T. Lan, H. Xiao, Y. Li, and J. Chen, "Enhanced current differential protection for HVDC grid based on Bergeron model: A parameter error tolerable solution," *IEEE Trans. Power Del.*, vol. 36, no. 3, pp. 1869–1881, Jun. 2021.
- [16] M. Davoudi, J. Sadeh, and E. Kamyab, "Transient-based fault location on three-terminal and tapped transmission lines not requiring line parameters," *IEEE Trans. Power Del.*, vol. 33, no. 1, pp. 179–188, Feb. 2018.
- [17] D. Lu, Y. Liu, Q. Liao, B. Wang, W. Huang, and X. Xi, "Time-domain transmission line fault location method with full consideration of distributed parameters and line asymmetry," *IEEE Trans. Power Del.*, vol. 35, no. 6, pp. 2651–2662, Dec. 2020.
- [18] J. Lita da Silva, "Strong consistency of least squares estimates in multiple regression models with random regressors," *Metrika*, vol. 77, no. 3, pp. 361–375, Apr. 2014.
- [19] M. Bockarjova, A. Sauhats, and G. Andersson, "Statistical algorithm for power transmission lines distance protection," in *Proc. Int. Conf. Probabilistic Methods Appl. Power Syst.*, Jun. 2006, pp. 96–105.
- [20] R. Prakash and E. Koley, "A combined Gabor transform-EKNN based protection scheme for AC-HVDC transmission line with DFIG wind turbine," in *Proc. 13th IEEE PES Asia-Pacific Power Energy Eng. Conf. (APPEEC)*, Thiruvananthapuram, India: IEEE, Nov. 2021, pp. 1–6.
- [21] H. Wang, X. Li, W. Zhou, and Y. Luo, "A pilot protection for transmission lines connected to wind power plants," in *Proc. IEEE Int. Conf. Adv. Power Syst. Autom. Protection (APAP)*, Xuchang, China: IEEE, Oct. 2023, pp. 558–561.
- [22] S. Biswas, B. K. Panigrahi, P. K. Nayak, G. Pradhan, and S. Padmanaban, "A single-pole filter-assisted improved protection scheme for the TCSC-compensated transmission line connecting large-scale wind farms," *IEEE J. Emerg. Sel. Topics Ind. Electron.*, vol. 5, no. 2, pp. 346–358, Apr. 2024.
- [23] P. K. Bera, V. Kumar, S. R. Pani, and O. P. Malik, "Autoregressive coefficients based intelligent protection of transmission lines connected to type-3 wind farms," *IEEE Trans. Power Del.*, vol. 39, no. 1, pp. 71–82, Feb. 2024.
- [24] Y. Yan, X. Chu, Q. Liu, H. Li, and L. Xu, "Process and protection action of commissioning fault of offshore wind farm grid-connected transmission lines," in *Proc. IEEE Int. Conf. Adv. Power Syst. Autom. Protection (APAP)*, Xuchang, China: IEEE, Oct. 2023, pp. 212–218.
- [25] N. Rezaei, M. N. Uddin, I. K. Amin, M. L. Othman, M. B. Marsadek, and Md. M. Hasan, "A novel hybrid machine learning classifier-based digital differential protection scheme for intertie zone of large-scale centralized DFIG-based wind farms," *IEEE Trans. Ind. Appl.*, vol. 56, no. 4, pp. 3453–3465, Jul. 2020.
- [26] S. Biswas and P. K. Nayak, "A new approach for protecting TCSC compensated transmission lines connected to DFIG-based wind farm," *IEEE Trans. Ind. Informat.*, vol. 17, no. 8, pp. 5282–5291, Aug. 2021.
- [27] A. K. Pradhan and G. Jos, "Adaptive distance relay setting for lines connecting wind farms," *IEEE Trans. Energy Convers.*, vol. 22, no. 1, pp. 206–213, Mar. 2007.
- [28] V. Yaramasu, B. Wu, P. C. Sen, S. Kouro, and M. Narimani, "High-power wind energy conversion systems: State-of-the-art and emerging technologies," *Proc. IEEE*, vol. 103, no. 5, pp. 740–788, May 2015.
- [29] P. Piya, M. Ebrahimi, M. Karimi-Ghartemani, and S. A. Khajehod-din, "Fault ride-through capability of voltage-controlled inverters," *IEEE Trans. Ind. Electron.*, vol. 65, no. 10, pp. 7933–7943, Oct. 2018.
- [30] N. Jabbar, E. Tsioumas, C. Mademlis, and E. Solomin, "A highly effective fault-ride-through strategy for a wind energy conversion system with a doubly fed induction generator," *IEEE Trans. Power Electron.*, vol. 35, no. 8, pp. 8154–8164, Aug. 2020.

- [31] B. Chen, A. Shrestha, F. A. Ituzaro, and N. Fischer, "Addressing protection challenges associated with type 3 and type 4 wind turbine generators," in *Proc. 68th Annu. Conf. Protective Relay Eng.*, Mar. 2015, pp. 335–344.
- [32] L. Zheng, K. Jia, W. Wu, Q. Liu, T. Bi, and Q. Yang, "Cosine similarity based line protection for large scale wind farms part II—The industrial application," *IEEE Trans. Ind. Electron.*, vol. 69, no. 3, pp. 2599–2609, Mar. 2022.
- [33] A. Saber, M. F. Shaaban, and H. H. Zeineldin, "A new differential protection algorithm for transmission lines connected to large-scale wind farms," *Int. J. Electr. Power Energy Syst.*, vol. 141, Oct. 2022, Art. no. 108220.
- [34] K. Jia, Z. Yang, L. Zheng, Z. Zhu, and T. Bi, "Spearman correlation-based pilot protection for transmission line connected to PMSGs and DFIGs," *IEEE Trans. Ind. Informat.*, vol. 17, no. 7, pp. 4532–4544, Jul. 2021.
- [35] S. Biswas, P. K. Nayak, and G. Pradhan, "A dual-time transform assisted intelligent relaying scheme for the STATCOM-compensated transmission line connecting wind farm," *IEEE Syst. J.*, vol. 16, no. 2, pp. 2160–2171, Jun. 2022.

LEI LI is currently an Engineer with State Grid Ningxia Electric Power Company Ltd., Electric Power Science Research Institute, Yinchuan, China. His research interest includes the control of wind-turbine generators.

JIANAN HE is currently an Engineer with State Grid Ningxia Electric Power Company Ltd., Electric Power Science Research Institute, Yinchuan, China. His research interests include power system protection and control.

JIAN NIU is currently an Engineer with State Grid Ningxia Electric Power Company Ltd., Electric Power Science Research Institute, Yinchuan, China. His research interests include modeling and simulation of wind turbines.

HAITAO LIU is currently an Engineer with State Grid Ningxia Electric Power Company Ltd., Electric Power Science Research Institute, Yinchuan, China. His research interests include modeling and simulation of power systems.

XIAOJUN YU is currently an Engineer with State Grid Ningxia Electric Power Company Ltd., Ningxia Power Supply Company, Yinchuan, China. His research interests include optimal power system control and analysis.

YING HUANG is currently an Engineer with State Grid Ningxia Electric Power Company Ltd., Yinchuan, China. His research interests include modeling and simulation of wind turbines.

XU ZHANG is currently an Associate Professor with China University of Mining and Technology, Beijing. His research interests include protection and control of renewable power systems.

• • •